



Case study on the dynamics of ultrafast laser heating and ablation of gold thin films by ultrafast pump-probe reflectometry and ellipsometry

T. Pflug¹ · J. Wang² · M. Olbrich¹ · M. Frank¹ · A. Horn¹

Received: 28 September 2017 / Accepted: 4 January 2018 / Published online: 11 January 2018
© Springer-Verlag GmbH Germany, part of Springer Nature 2018

Abstract

To increase the comprehension of ultrafast laser ablation, the ablation process has to be portrayed with sufficient temporal resolution. For example, the temporal modification of the complex refractive index \tilde{n} and the relative reflectance of a sample material after irradiation with ultrafast single-pulsed laser radiation can be measured with a pump-probe setup. This work describes the construction and validation of a pump-probe setup enabling spatially, temporally, and spectroscopically resolved Brewster angle microscopy, reflectometry, ellipsometry, and shadow photography. First pump-probe reflectometry and ellipsometry measurements are performed on gold at $\lambda_{\text{probe}} = 440$ nm and three fluences of the single-pulsed pump radiation at $\lambda_{\text{pump}} = 800$ nm generating no, gentle, and strong ablation. The relative reflectance overall increases at no and gentle ablation. At strong ablation, the relative reflectance locally decreases, presumably caused by emitted thermal electrons, ballistic electrons, and ablating material. The refractive index n is slightly decreasing after excitation, while the extinction coefficient k is increasing.

1 Introduction

The comprehension of the dynamics of ultrafast laser ablation is becoming more and more important due to rising demands for microtechnics, like thin-film electronics [1]. Therefore, the laser ablation has to be characterized consistently with sufficient temporal resolution. The temporal and spatial modification of the complex refractive index \tilde{n} and the reflectance R of a material after irradiation with ultrafast laser radiation represent physical parameters, which can be measured with high temporal resolution combining a pump-probe setup with an ellipsometer [2]. This article explains the fundamentals of ellipsometry with rotating analyzer [3, 4] and describes the construction of an automated pump-probe setup enabling spatially, temporally, angularly,

and spectroscopically resolved pump-probe ellipsometry, reflectometry, Brewster angle microscopy, and shadow photography. First results of pump-probe reflectometry at no ablation, gentle ablation and strong ablation, and pump-probe ellipsometry below ablation threshold are presented and discussed.

2 Ellipsometry with rotating analyzer

Ellipsometry determines the change of the polarization of radiation after its reflection on a sample surface. The electrical field strength of the radiation after the reflection $E_{\text{ref},\parallel/\perp}$ on an interface of two media is described by the reflection coefficients r_{\parallel} for the parallel and r_{\perp} for the orthogonal component of the electrical field strength from the Fresnel equations:

$$E_{\text{ref},\parallel/\perp} = E_{\text{inc},\parallel/\perp} \cdot r_{\parallel/\perp}, \quad (1)$$

with the incident electrical field strength $E_{\text{inc},\parallel/\perp}$. The complex ratio of the reflection coefficients:

$$\rho = \frac{r_{\parallel}}{r_{\perp}} = \tan \Psi \cdot e^{i\Delta} \quad (2)$$

The original version of this article was revised: Several terms on the pages 3, 4, 5, and 7 were incorrect.

✉ A. Horn
horn4@hs-mittweida.de

¹ Laserinstitut Hochschule Mittweida, Technikumplatz 17, 09648 Mittweida, Germany

² Ruhr-Universität Bochum, Laser and Photonics, Universitätsstraße 150, 44801 Bochum, Germany

characterizes the change of the amplitude ratio and the phase difference of the reflected radiation. This change is caused by the optical properties of the irradiated material and is expressed by the ellipsometric parameters Δ and Ψ [3, 4]. In this work, ellipsometry with rotating analyzer (Fig. 1) is applied to measure these two parameters. The electromagnetic radiation is emitted by a source (M) at a certain wavelength with small bandwidth and the polarization state is defined using a polarizer (P) with the angle φ relative to the incident plane. The radiation propagates through an ambient medium with the complex refractive index \tilde{n}_0 and is reflected with the angle of incidence θ on a sample surface (S) with the complex refractive index \tilde{n}_1 . A camera (D) detects the intensity distribution I of the reflected radiation depending on the angle ϕ of a rotating analyzer (A) (Fig. 2). The intensity distribution I can be described by an approximated function with a periodicity of 180°:

$$I(\phi) = I_0 \cdot [1 + \alpha \cdot \cos(2\phi) + \beta \cdot \sin(2\phi)], \quad (3)$$

with the normalization factor I_0 and the coefficients α and β , representing the amplitude and phase of the approximated function. Setting $\varphi = 45^\circ$, the ellipsometric parameters Δ and Ψ can be directly obtained by the following [3–5]:

$$\Delta = \arccos\left(\frac{\beta}{\sqrt{1 - \alpha^2}}\right), \quad \text{and} \quad (4)$$

$$\Psi = \arctan\left(\sqrt{\frac{1 + \alpha}{1 - \alpha}} \cdot \tan(|\varphi|)\right). \quad (5)$$

Knowing the ellipsometric parameters Δ and Ψ and the angle of incidence θ of the radiation, the complex refractive index \tilde{n}_1 of the sample material can be calculated by the dielectric function ϵ with [3, 4]:

$$\tilde{n}_1 = \sqrt{\epsilon} = \tilde{n}_0 \sin(\theta) \sqrt{1 + \left(\frac{1 - \rho}{1 + \rho}\right)^2 \tan^2(\theta)}. \quad (6)$$

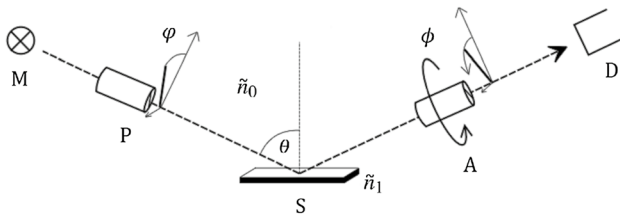


Fig. 1 Principle of ellipsometry with rotating analyzer: radiation source M, polarizer P, polarization angle φ , complex refractive index of ambient medium \tilde{n}_0 , angle of incidence θ , sample material S, complex refractive index of sample material \tilde{n}_1 , analyzer A, analyzer angle ϕ , detector D

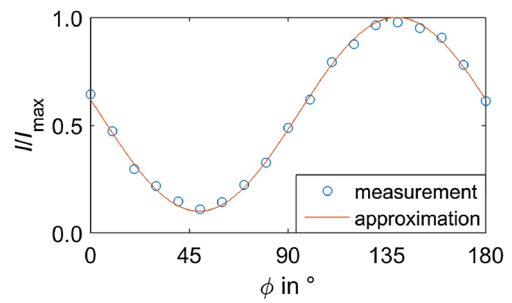


Fig. 2 Measured normalized intensity I of the reflected probe radiation on gold depending on the analyzer angle ϕ and associated approximated function $I(\phi)$

3 Materials and methods

3.1 Experimental setup

In principle, a pump-probe setup requires pump radiation, which excites the sample material and probe radiation which detects the induced modifications of the optical parameters. Therefore, the applied laser radiation, provided by an amplified Ti:sapphire laser system (Astrella, Coherent Inc., (1), $\lambda = 800\text{nm}$, $\tau_H = 35\text{fs}$, $M^2 = 1.2$), is divided by a beam splitter into pump (*red*) and probe (*blue*) radiation (Fig. 3). The wavelength of the pump radiation is set to $\lambda_{\text{pump}} = 800\text{nm}$, while the wavelength of the probe radiation can be changed in the range $240\text{nm} < \lambda_{\text{probe}} < 20\text{ }\mu\text{m}$ using an optical parametric amplifier [TOPAS Prime, Light Conversion Inc., (2)]. First measurements are accomplished at $\lambda_{\text{probe}} = 440\text{nm}$ enabling a separation of both radiations. The temporal separation of the pump radiation relative to the probe radiation is variable in the range of $-500\text{ps} < \Delta t < 4\text{ns}$ using a delay stage (3). The pump radiation is focused on the sample material by a plan convex

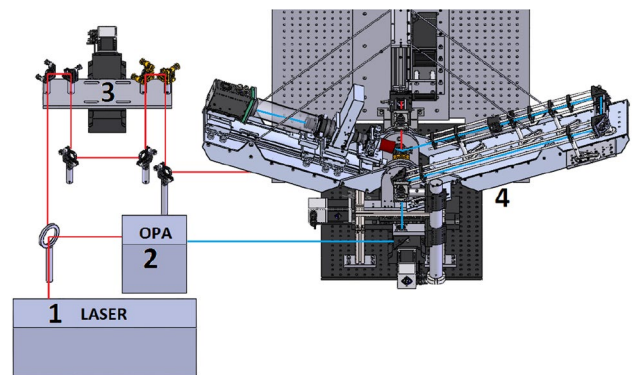


Fig. 3 Schematic experimental setup: (1) radiation source, (2) optical parametric amplifier, (3) delay stage varying the optical path length of the pump radiation (red) relative to the optical path length of the probe radiation blue, and (4) pump-probe setup

lens ($f = 150$ mm) resulting in modifications of the optical parameters by heating, melting, and ablating the material. The polarization of the probe radiation is completely linear and aligned to $\varphi = 45^\circ$ relative to the incident plane by a polarizer. Finally, the probe radiation is reflected on the sample material at the angle of incidence θ , and spatially resolved detected by an imaging system consisting of an objective, an analyzer, a tube lens, and a CCD camera (GE 1024 1024 BI UV3, greateyes GmbH) with a calculated spatial resolution of $\Delta x = \Delta y = 0.65$ μm . The angle of incidence of the probe radiation is tunable in the range of $55^\circ < \theta < 90^\circ$. To block scattered pump radiation and inhibiting the optical plasma emission, a Fabry-Pérot filter is placed inside the imaging system. Due to the group velocity dispersions of the optical elements, the pulse durations of the pump and probe radiation are increased, resulting in $\tau_{H,pump} = 40$ fs and $\tau_{H,probe} = 60$ fs at the sample surface measured by an autocorrelator. The spatial intensity distribution of the pump radiation is almost Gaussian with a focused beam radius $w_{0,pump} = 18$ μm on the sample surface and is completely overlapped by the probe radiation with $w_{0,probe} = 400$ μm . The pulse energy of the pump radiation can be automatically changed by an external attenuator enabling pulse energies in the range of 0.1 $\mu\text{J} < Q_{p,pump} < 65$ μJ . The pump-probe setup additionally enables reflectometry, Brewster angle microscopy, and shadow photography by removing the analyzer.

3.2 Characterisation of the sample material

All pump-probe experiments are performed with single-pulsed laser radiation on gold thin films on top of a fused silica substrate with a layer thickness $d_{gold} = 200$ nm and a roughness $R_{a,gold} = (2.7 \pm 0.8)$ nm. The optical penetration depth d_p is smaller than 20 nm for radiation at 240 nm $< \lambda_{probe} < 20$ μm .

Ablating material with ultrafast pulsed laser radiation, two different ablation regimes are observed depending on the fluence of the radiation. At low fluences, the material is only heated after irradiation and no change of the material surface is detected by SEM and confocal microscopy implying a reversible process (Fig. 4, left column). At fluences in the gentle regime, the material is ablated by spallation and phase explosion [6] (Fig. 4, middle column, area 1), and at fluences in the strong regime, the border area (area 1) of the irradiated material is ablated by phase explosion, while in the center critical point, phase separation occurs [6] (Fig. 4, right column, area 2). The pump-probe reflectometry is performed at different peak fluences H_0 to investigate the different ablation regimes. The threshold fluences:

$$H_{thr} = \frac{2Q_{p,thr}}{\pi w_{0,pump}^2} \tag{7}$$

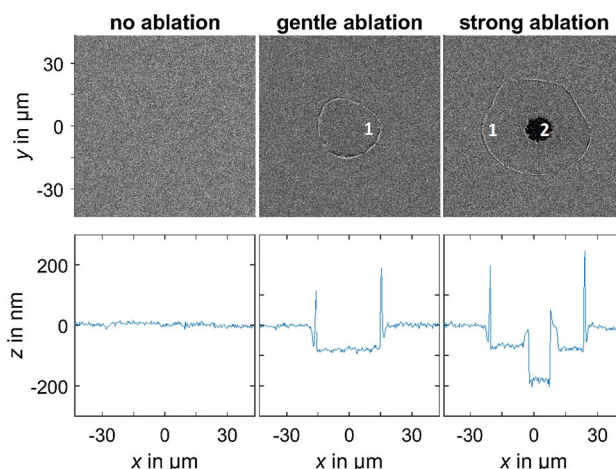


Fig. 4 Top: structures generated by single-pulsed pump radiation detected by SEM (left: $H_0 < H_{thr,gentle}$, middle: $H_{thr,gentle} < H_0 < H_{thr,strong}$, right: $H_0 > H_{thr,strong}$); bottom: cross section of the generated structures detected by confocal microscopy

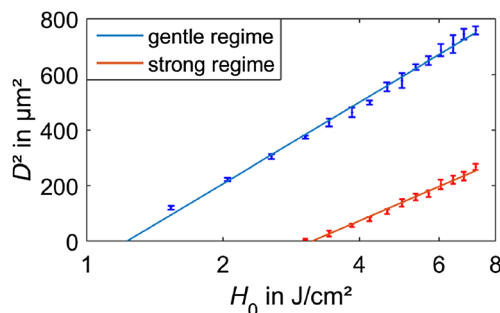


Fig. 5 Squared diameter of the structures generated by single-pulsed pump radiation depending on the fluence of the pump radiation for gentle and strong ablation (Liu plot [17])

of gold for gentle and strong ablation are determined by Liu plot [17]. The structure diameters were detected by confocal microscopy by forming the arithmetic mean of the diameters of five generated structures each (Fig. 5). The resulting threshold fluences for gentle and strong ablation are $H_{thr,gentle} = (1.2 \pm 0.5) \frac{\text{J}}{\text{cm}^2}$ and $H_{thr,strong} = (3.2 \pm 0.6) \frac{\text{J}}{\text{cm}^2}$.

4 Experimental results and discussion

4.1 Pump-probe reflectometry

A change of the relative reflectance:

$$\Delta R/R = \frac{R_{ir} - R}{R} \tag{8}$$

of a sample material is caused by laser induced heating, melting, evaporation, and plasma formation, with the reflectance before R and after irradiation R_{ir} .

First, spatially and temporally resolved pump-probe reflectometry measurements are accomplished on gold by targeting single-pulsed pump and probe radiation at different fluences of the pump radiation. The wavelengths of the pump and probe radiations are set to $\lambda_{pump} = 800$ nm and $\lambda_{probe} = 440$ nm and the angle of incidence to $\theta = 60^\circ$. The fluence of the pump radiation is chosen to three values:

1. below the threshold fluence for gentle regime $H_0 = 1 \frac{J}{cm^2}$.
2. between the threshold fluences for gentle and strong regime $H_0 = 2 \frac{J}{cm^2}$.
3. above the threshold fluence for strong regime $H_0 = 7 \frac{J}{cm^2}$.

The minimum time step of the pump radiation relative to the probe radiation is set to $\Delta t = 0.2$ ps. The time step, indicating a first relative reflectance change, is defined as $t = 0$ ps. Before irradiating the sample material, the relative reflectance $\Delta R/R$ does not change and remains zero (Fig. 6, left column). Below the gentle regime, no ablation or modification is detected by SEM, whereas in the gentle regime, a constant ablation depth of about 80 nm is detected. In the strong regime, the thin gold film is completely removed in the center of the irradiated area down to the substrate, and ablated about 80 nm in depth in the border area of the

irradiated area [18] (Fig. 4, bottom row; and Fig. 6, right column). The detected morphology resembles other investigations and might be explained by homogeneous nucleation [7, 19, 20].

For all three ablation regimes, the spatially extent of the change of the relative reflectance reaches its maximum directly after irradiation and decreases steadily afterwards (Fig. 7, top). At all ablation regimes, the changes of the relative reflectance increase within $0 \text{ ps} < t < 1 \text{ ps}$ and reach almost the same maximum of $\Delta R/R \approx 1$ (Fig. 7, bottom). For no and gentle ablation, the change of the relative reflectance decreases approximately exponential at $t > 1$ ps. Exciting gold without ablation, the relative reflectance almost relaxes, while $\Delta R/R$ at gentle regime after $t > 500$ ps begins to fluctuate. The positive change of the relative reflectance of gold after irradiation is based on the evolution of the density of states of the s , p , and d band electrons of gold and the heating of the material caused by the pump radiation. The conduction band of gold is formed by the s and p electrons and the valence band is formed by the d electrons. The interband transition threshold (ITT) to excite electrons from the d into the s band is calculated to $E_{ITT} = 2.47$ eV corresponding to a wavelength $\lambda_{ITT} \approx 500$ nm [14, 16]. At rest, probe radiation at $\lambda_{probe} < \lambda_{ITT}$, consequently $E > E_{ITT}$, is absorbed exciting electrons from the d to the s band, while radiation at $\lambda_{probe} > \lambda_{ITT}$ does not excite electrons and is reflected resulting in a higher reflectance

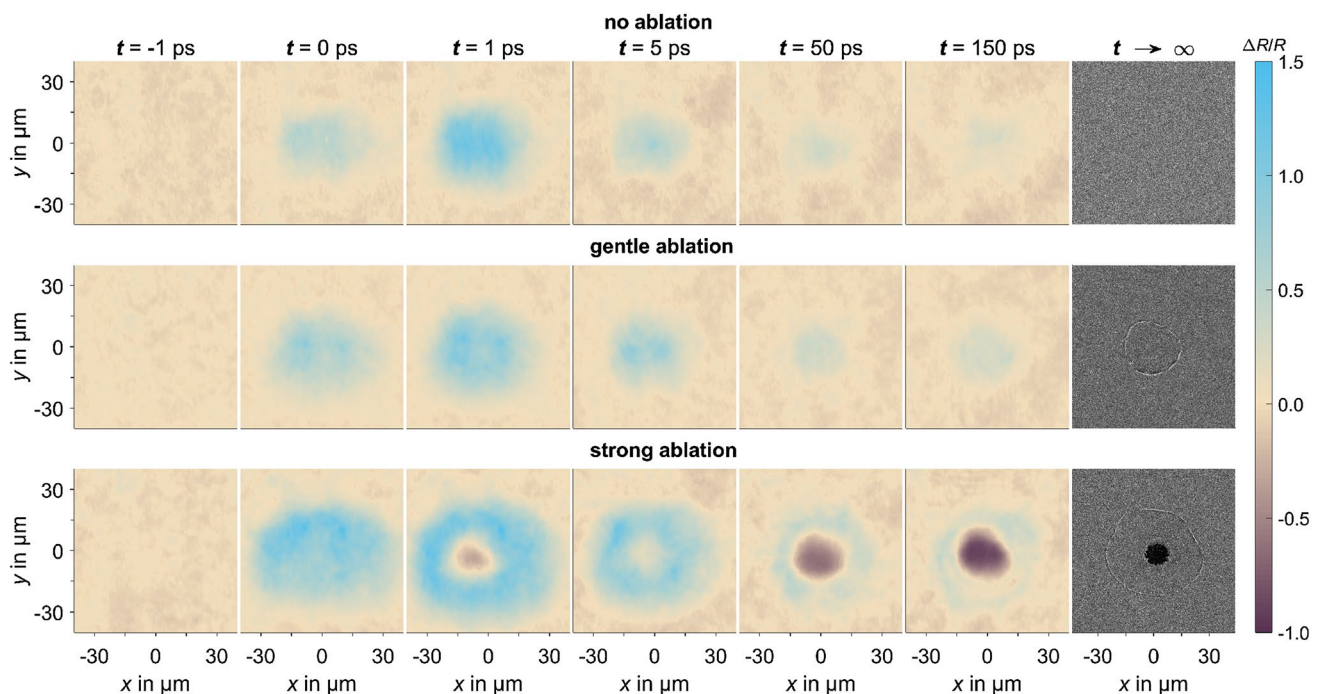


Fig. 6 Left: Spatially resolved change of the relative reflectance of gold after irradiation with single-pulsed pump radiation without ablation (top row), gentle ablation (middle row), and strong ablation (bot-

tom row) at different delay times; right column: Generated structures detected by SEM

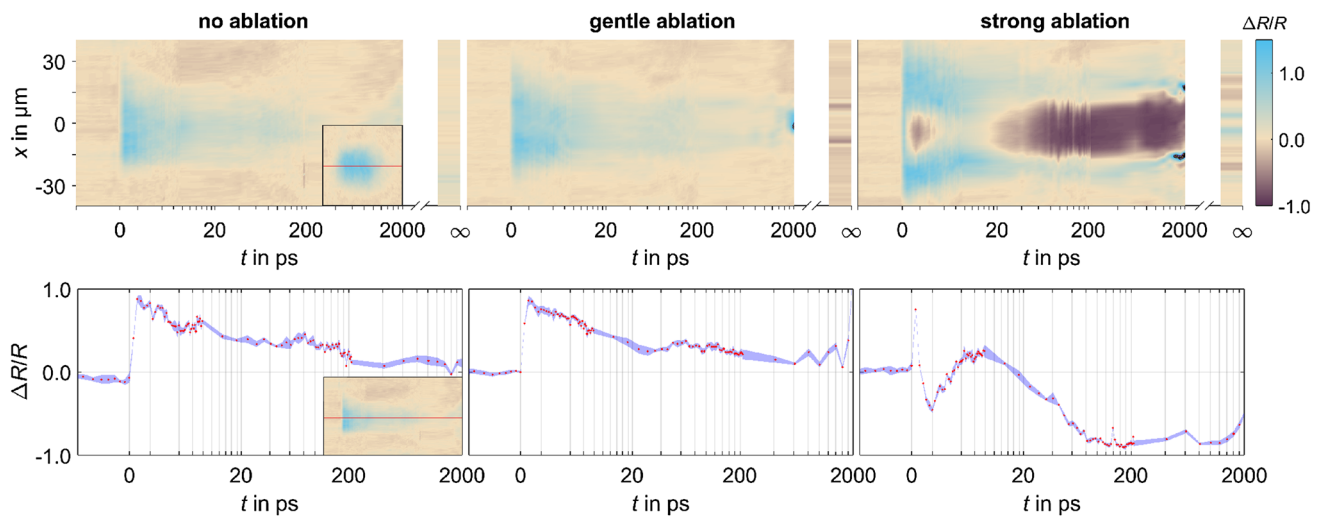


Fig. 7 Top: cross section on the y-axis of the spatially resolved change of the relative reflectance plotted as function of the delay time (see inlet); bottom: relative reflectance at one spatial point plotted as function of the delay time (see inlet)

$R(\lambda_{\text{probe}} > \lambda_{\text{ITT}}) > R(\lambda_{\text{probe}} < \lambda_{\text{ITT}})$. Only transitions keeping the conservation of energy and momentum are allowed. Because the momentum of a single photon can be neglected compared to the momentum of an electron, the excited electrons approximately maintain their momentum [13–16]. Heating the electrons at energies below the Fermi level of the sample material with single-pulsed pump radiation, this electrons are excited into states above the Fermi level resulting in less free states in the s band. Thereby, photons of the probe radiation at $\lambda_{\text{probe}} < \lambda_{\text{ITT}}$ can excite less electrons from the d into the s band, because there are less free states above the Fermi level available [13, 14, 16], wherefore less photons are absorbed and the relative reflectance is increasing (Fig. 7, left column and middle column).

For strong ablation, the maximum of $\Delta R/R$ is slightly lower than for no and gentle ablation, possibly caused by the applied temporal resolution. The change of the relative reflectance in the center of the irradiated area abruptly decreases to $\Delta R/R = -0.5$ at $t = 2$ ps possibly evoked by thermal electron emission from the material surface [21] and non-equilibrium ballistic electrons propagating in all directions caused by excitation [12, 14, 16]. The spatially extent of this center area resembles to the extent of the strong ablation of the structure (Fig. 6). Afterwards up to $t = 10$ ps, the relative reflectance increases to $\Delta R/R = 0.25$ due to thermalization of the electron and phonon systems and gaining an equilibrium [20]. The subsequently decrease of the relative reflectance to $\Delta R/R = -0.8$ at $10 \text{ ps} < t < 80 \text{ ps}$, persisting till $t = 500$ ps (Fig. 7, right column) could be explained by the heated phonon system and following phase changes and ablation [22], since the density and the optical properties of the material are modified during phase changes [24]. At $t > 20$ ps, the material surface possibly begins to bulge [9] and

the relative reflectance decreases to a minimum of -0.8 at $t > 80$ ps due to the complete ablation of the thin gold film down to the substrate material as molecular dynamic simulations show [8, 11]. The molecular dynamic simulations consider the ablation as a one-dimensional process. In reality, the arising vapor and particulates have a lateral extension, whereby the area with decreased relative reflectance is significantly greater than the area of the strong ablation of the structure (Fig. 6). The temporally resolved evolution of the relative reflectance $\Delta R/R$ in the border area $|y| > 20 \mu\text{m}$ for strong ablation (Fig. 7, right column) resembles those of the cases of no and gentle ablation.

4.2 Pump-probe ellipsometry

The validation of the pump-probe ellipsometer is achieved by comparative measurements of Δ and Ψ on gold samples at rest depending on the wavelength with a commercial ellipsometer (nanofilm_ep4, Accurion GmbH) and literature measurements [10] (Fig. 8, left).

The measured ellipsometric parameters Δ and Ψ and the Eq. (6) calculated refractive index n and extinction coefficient k (Fig. 8, right) yield a deviation from the literature less than 10%. The angle of incidence was set to $\theta = 60^\circ$.

First, pump-probe ellipsometry measurements are accomplished spatially and temporally resolved for gold with single-pulsed pump ($\lambda = 800 \text{ nm}$, $\tau_{\text{H}} = 40 \text{ fs}$) and probe ($\lambda = 440 \text{ nm}$, $\tau_{\text{H}} = 60 \text{ fs}$) radiation. The fluence of the pump radiation is set below the threshold fluence for gentle ablation of gold at $H_0 = 1 \frac{\text{J}}{\text{cm}^2}$. The minimum time step of the pump radiation relative to the probe radiation is set to $\Delta t = 40 \text{ fs}$ with a maximum temporal delay range of 1.5 ps. The ellipsometric parameters Δ and Ψ of gold abruptly increase

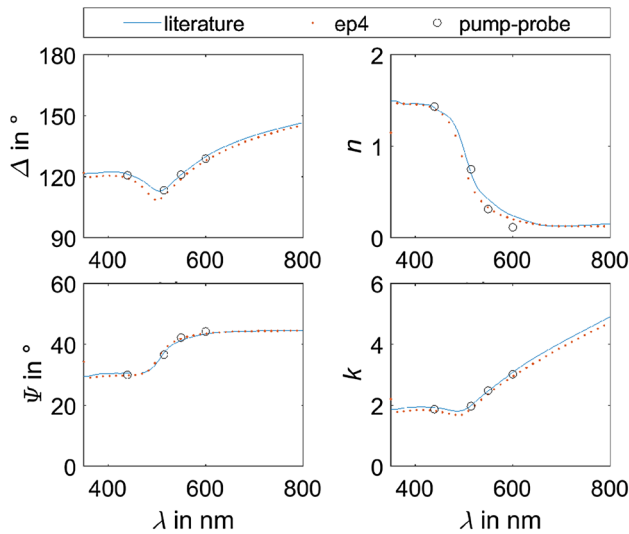


Fig. 8 left: Comparison of the ellipsometric parameters Δ and Ψ measured by the self-developed ellipsometer, measured by a commercial ellipsometer (nanofilm_ep4, Accurion GmbH), and literature values [10] of gold at rest, right: Comparison of n and k derived by Eq. (6) from Δ and Ψ measured by the pump-probe and a commercial ellipsometer and literature values [10] of gold without excitation

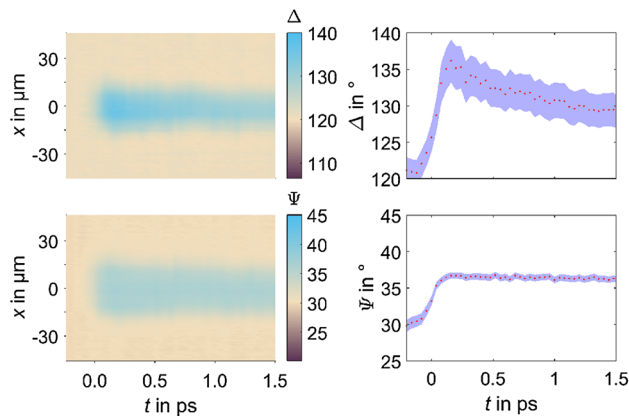


Fig. 9 Left: Cross section on the y-axis of the spatially resolved ellipsometric parameters Δ and Ψ plotted as function of the delay time after irradiation with single-pulsed pump radiation without ablation; right: ellipsometric parameters Δ and Ψ at one spatial point $x = 0 \mu\text{m}$ plotted as function of the delay time

after irradiation (Fig. 9, right). Δ reaches its maximum of $\Delta = 136^\circ$ within the first 200 fs and decreases steadily to $\Delta = 129^\circ$ afterwards. Ψ increases to its maximum of $\Psi = 36^\circ$ during $0 \text{ fs} < t < 200 \text{ fs}$ and persists up to $t = 1.5 \text{ ps}$. The spatially extent of the modified area increases to $\Delta y \approx 30 \mu\text{m}$ at $0 \text{ ps} < t < 0.2 \text{ ps}$ and remains almost constant the whole considered time range (Fig. 9, left).

The comparison of $\Delta R/R$ calculated from the measured ellipsometric parameters Δ and Ψ by Eq. (2) and (6) with

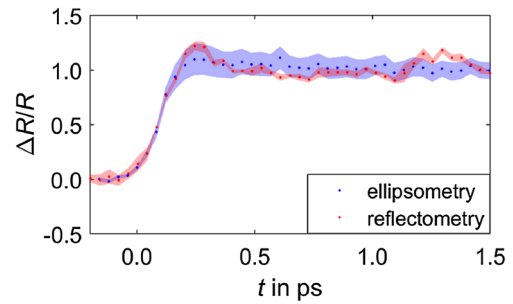


Fig. 10 Comparison of the change of the relative reflectance $\Delta R/R$ of gold as function of time calculated from the measured ellipsometric parameters Δ and Ψ with the measured change of the relative reflectance $\Delta R/R$ of gold

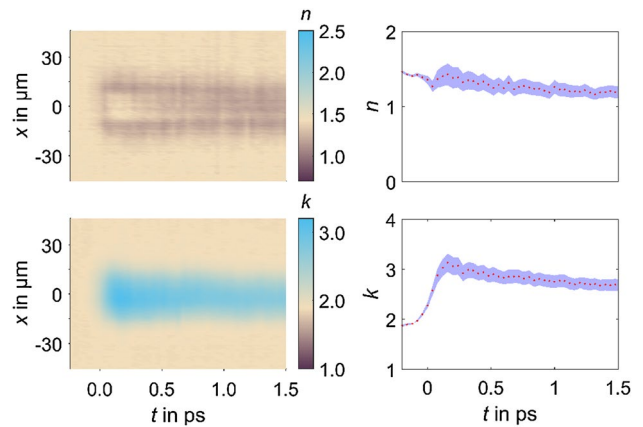


Fig. 11 Left: temporally resolved refractive index n and extinction coefficient k of gold derived by Eq. (6) plotted as function of the delay time after irradiation with single-pulsed pump radiation without ablation; right: refractive index n and extinction coefficient k at one spatial point $x = 0 \mu\text{m}$ plotted as function of the delay time

the previous measurements of $\Delta R/R$ from Sect. 4.1 reveals a relative deviation less than 10% (Fig. 10).

The gained information of Δ and Ψ is derived from the first few nanometers in depth of the thin gold film given by the optical penetration depth d_p of the probe radiation. Without excitation with pump radiation, the optical penetration depth of the probe radiation at $\lambda_{\text{probe}} = 440 \text{ nm}$ is calculated to $d_p \approx 18 \text{ nm}$. After excitation with pump radiation, the optical properties of the material change. As a first approach, any possible arising gradients in depth of the thermophysical properties of the material caused by irradiation are neglected, and the irradiated area is considered homogeneous and given by an effective medium [3, 23]. Therefore, the temporally and spatially resolved refractive index n and extinction coefficient k of the material can be calculated by Eq. (6) (Fig. 11). At rest, the optical properties of gold are $n = 1.5$ and $k = 1.9$. After irradiation, the refractive index n decreases to a local minimum of $n = 1.25$ at 0

$ps < t < 0.1$ ps, locally increases again to $n = 1.4$ at 0.1 ps $< t < 0.25$ ps, and steadily decreases afterwards to $n = 1.2$ in the investigated time range. The extinction coefficient k abruptly increases to $k = 3.1$ at 0 ps $< t < 0.2$ ps and steadily decreases to 2.7 in the considered time range.

5 Summary and outlook

An automated pump-probe setup combined with an ellipsometer enabling temporally, spatially, angularly, and spectroscopically resolved ellipsometry, reflectometry, Brewster angle microscopy, and shadow photography was constructed and validated. Pump laser radiation at $\lambda_{\text{pump}} = 800$ nm and $\tau_{\text{H,pump}} = 40$ fs and probe laser radiation at 240 nm $< \lambda_{\text{probe}} < 20$ μm and $\tau_{\text{H,probe}} = 60$ fs are applied. The ellipsometer is based on the rotating analyzer method measuring the ellipsometric parameters Δ and Ψ representing the change of the polarization of the probe radiation due to the reflection on a sample material. The self-developed ellipsometer is validated by comparing the spectroscopically ellipsometric parameters Δ and Ψ measured by the self-developed with those of a commercial ellipsometer, and literature values [10].

First, pump-probe reflectometry measurements were accomplished at $\lambda_{\text{probe}} = 440$ nm and a temporal range of 0 ns $\leq t \leq 2$ ns with $\Delta t_{\text{min}} = 200$ fs at different fluences of the single-pulsed pump radiation to examine different ablation regimes, the so-called gentle and strong regimes. The change of the relative reflectance of gold after irradiation is overall positive for no and gentle ablation regimes, which can be explained by the interband transition threshold of gold, and the broadening of the Fermi distribution by heating the metal. For strong ablation, the change of the relative reflectance is locally decreasing due to possibly emitting thermal electrons from the surface, propagating ballistic electrons, bulging of the surface of the material, and ablating material expanding into space.

First, pump-probe ellipsometry measurements were performed at $\lambda_{\text{probe}} = 440$ nm and a temporal range of -0.5 ps $\leq t \leq 1.5$ ps with $\Delta t_{\text{min}} = 40$ fs without ablation at the fluence $H_{0,\text{no}} = 1 \frac{\text{J}}{\text{cm}^2}$ of the single-pulsed pump radiation. The measured ellipsometric parameters Δ and Ψ of gold are both increasing after irradiation. The complex refractive index \tilde{n} of gold was calculated, assuming a homogeneous change of the thermophysical properties. The refractive index n is slightly decreasing after irradiation, whereas the extinction coefficient k of gold is heavily increasing.

To interpret the measured ellipsometric parameters Δ and Ψ more precise, further models have to account the possibly arising gradients of the thermophysical and optical properties in depth of the sample material caused by laser radiation.

Acknowledgements The authors gratefully acknowledge the financial support of the joint project no. 8222501 from the Staatsministerium für Wissenschaft und Kunst (SMWK).

References

1. K. Sugioka, *Ultrafast Laser Processing: From Micro- to Nanoscale: From Micro- to Nanoscale* (CRC Press, Hoboken, 2013)
2. A. Horn, *Ultra-Fast Material Metrology* (Wiley-VCH, Weinheim, 2009)
3. H. Fujiwara, *Spectroscopic Ellipsometry* (Wiley, Chichester, UK, 2007)
4. H.G. Tompkins (ed.), *Handbook of Ellipsometry* (Andrew, Norwich, 2010)
5. S. Rapp, M. Kaiser, M. Schmidt, H.P. Huber, *Opt. Express* **24**, 17572 (2016)
6. C. Cheng, X. Xu, *Phys. Rev. B* **72**, 165415 (2005)
7. R.D. Murphy, B. Torralva, S.M. Yalisove, *Appl. Phys. Lett.* **102**, 181602 (2013)
8. D.S. Ivanov, V.P. Lipp, V.P. Veiko, E. Yakovlev, B. Rethfeld, M.E. Garcia, *Appl. Phys. A* **117**, 2133 (2014)
9. K.J. Schrider, B. Torralva, S.M. Yalisove, *Appl. Phys. Lett.* **107**, 124101 (2015)
10. P.B. Johnson, R.W. Christy, *Phys. Rev. B* **6**, 4370 (1972)
11. Z. Lin, E. Leveugle, E.M. Bringa, L.V. Zhigilei, *J. Phys. Chem. C* **114**, 5686 (2010)
12. X. Liu, R. Stock, W. Rudolph, in *Conference on Lasers and Electro-Optics/International Quantum Electronics Conference and Photonic Applications Systems Technologies* (OSA Washington, D.C., 2004), IWA4
13. C.-K. Sun, F. Vallée, L.H. Acioli, E.P. Ippen, J.G. Fujimoto, *Phys. Rev. B* **50**, 15337 (1994)
14. S.-S. Wellershoff, J. Hohlfeld, J. Güdde, E. Matthias, *Appl. Phys. A* **69**, S99–S107 (1999)
15. C. Kittel, *Introduction to Solid State Physics* (Wiley, Hoboken, 2011)
16. S.-S. Wellershoff, *Untersuchungen zur Energierelaxationsdynamik in Metallen nach Anregung mit ultrakurzen Laserpulsen* (PhD thesis, Berlin, 2000)
17. J.M. Liu, *Opt. Lett.* **7**, 196 (1982)
18. M. Olbrich, E. Punzel, R. Roesch, R. Oettking, B. Muhsin, H. Hoppe, A. Horn, *Appl. Phys. A* **122**, 648 (2016)
19. N.A. Inogamov, V.A. Khokhlov, Y.V. Petrov, V.V. Zhakhovsky, K.P. Migdal, D.K. Ilnitsky, N. Hasegawa, M. Nishikino, M. Yamagiwa, M. Ishino, T. Kawachi, A.Y. Faenov, T.A. Pikuz, M. Baba, Y. Minami, T. Suemoto, in *Shock Compression of Condensed Matter: Proc. of Conf. of APS, Topical Group on Shock Compression of Condensed Matter*, 70012 (2017)
20. M. Olbrich, E. Punzel, P. Lickschat, S. Weißmantel, A. Horn, *Phys. Procedia* **83**, 93 (2016)
21. W. Wendelen, B.Y. Mueller, D. Autrique, B. Rethfeld, A. Bogaerts, *J. Appl. Phys.* **111**, 113110 (2012)
22. J. Wei, Z. Sun, F. Zhang, W. Xu, Y. Wang, F. Zhou, F. Gan, *Chem. Phys. Lett.* **392**, 415 (2004)
23. T.C. Choy, *Effective medium theory: Principles and applications: Principles and applications* (Clarendon Press, Oxford, 2007)
24. K. Sokolowski-Tinten, J. Bialkowski, M. Boing, A. Cavalleri, D. von der Linde, *Phys. Rev. B* **58**, R11805–R11808 (1998)